Core–Shell Nanoparticles

DOI: 10.1002/anie.200907019

PtSn Intermetallic, Core–Shell, and Alloy Nanoparticles as CO-Tolerant Electrocatalysts for H_2 Oxidation**

*Zhufang Liu, Greg S. Jackson, and Bryan W. Eichhorn**

The poisoning of Pt electrocatalysts by carbon monoxide (CO), a major impurity in H_2 fuels derived from reformed hydrocarbons, limits the commercialization of Nafion-based proton-exchange membrane (PEM) fuel cells.[1] To mitigate the CO-poisoning effect in PEM fuel cells, one straightforward strategy is to replace Pt with Pt-based bimetallic electrocatalysts that can tolerate small amounts of CO (typically <100 ppm). Three promising classes of Pt-based bimetallic NPs have been investigated for this purpose: 1) Pt–M alloys (e.g. PtRu) with metal atoms randomly distributed in face-centered-cubic (fcc) lattices,[2–4] 2) ordered intermetallics (e.g. PtBi) that have well-defined compositions and crystal structures,[5] and 3) core–shell bimetallics, e.g. Ru-core/Pt-shell (Ru@Pt) in which Pt is concentrated on the Ru nanoparticle surface.[6] Each of these bimetallic architectures has potential advantages and disadvantages in terms of synthetic accessibility, performance, and stability in electrocatalytic applications. However, a direct comparison of these three architectures in a specific Pt–M series has not been reported.

We describe here the synthesis, characterization, electrocatalytic performance, and stabilities of PtSn alloy, core–shell, and intermetallic nanoparticles (NPs) of the same composition and size. These studies show that the PtSn intermetallic is significantly more stable and has superior performance relative to the PtSn alloy in acidic electrolyte solutions. In addition, the intermetallic can be converted to a PtSn@Pt core–shell particle through a successive potential cycling process in CO-saturated H_2SO_4 solutions, while no such core–shell structure forms from PtSn random alloys. The PtSn@Pt and PtSn intermetallic NP electrocatalysts show significantly better CO -tolerance than commercial E-TEK PtRu and Pt catalysts but presumably involve different CO oxidation mechanisms.

PtSn intermetallic NPs were prepared by the co-reduction of $[Pt(acac)_2]$ (acac = acetylacetonate) and $SnCl_4$ in octadecene by using $NaBEt_3H$, a strong reducing agent. Oleylamine and oleic acid were employed as capping agents to control the particle size and shape. The transmission electron microscopy (TEM) image of as-prepared NPs (Figure 1a) shows the particles have an average size of 3.5 nm with a narrow size distribution. To make electrocatalysts, the as-prepared intermetallic particles were loaded onto carbon supports and subsequently heated at 450 °C in Ar/H_2 (5% H_2) to remove the capping agents. Despite the high annealing temperatures, no significant particle growth or aggregation was observed. Most of the post-treated NPs were still in the size range of 3–5 nm, with only a few particles larger than 5 nm (Figure 1b). The NP lattice fringes (insert of Figure 1b) show an average lattice separation of 0.21 nm, which corresponds to the (102) plane of the hexagonal ($P6_3/mmc$) PtSn intermetallic. The X-ray diffraction (XRD) pattern of the intermetallic catalyst (Figure 1c) displays the distinct hexagonal pattern associated with the PtSn intermetallic. Single-particle TEM-EDX line scans show Gaussian distributions of Pt and Sn across the particle (Figure 1d), indicating that the NPs are bimetallic in nature with homogenous distributions of elements.

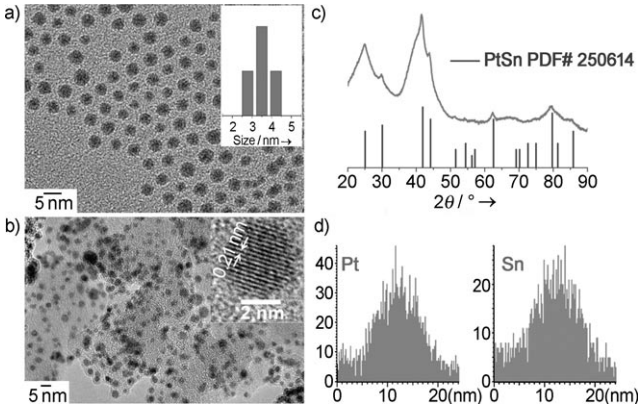

Figure 1. a) TEM image of as-prepared PtSn intermetallic NPs. The insert is the size distribution histogram; b) TEM image and lattice fringe image (insert) of carbon-supported PtSn intermetallic NPs; c) XRD profile of PtSn intermetallic catalysts; d) TEM-EDX line scan of one PtSn intermetallic NP.

PtSn random alloy NPs were also prepared by the co-reduction of $[Pt(acac)_2]$ and $SnCl_4$, but ethylene glycol and polyvinyl-pyrrolidone (PVP) were used as the solvent and capping agent, respectively. The NPs have an average particle size of 4.0 nm (Supporting Information, Figure S1a). XRD profiles of the particles show an fcc crystal structure

[*] Dr. Z. Liu, Prof. B. W. Eichhorn
Department of Chemistry & Biochemistry, University of Maryland
College Park, MD 20742 (USA)
Fax: (+1) 301-314-9121
E-mail: eichhorn@umd.edu
Prof. G. S. Jackson
Department of Mechanical Engineering, University of Maryland
College Park, MD 20742 (USA)

[**] This work was supported by U.S. Department of Energy HFI program (Grant No. DE-FG02-05ER15731) and the University of Maryland Energy Research Center (UMERC). We acknowledge the support of the Maryland NanoCenter, which is supported in part by the NSF as a MRSEC Shared Experimental Facility.

Supporting information for this article is available on the WWW under http://dx.doi.org/10.1002/anie.200907019.

(Figure S1b). However, the diffraction peaks are shifted to lower 2θ values compared with those of fcc monometallic Pt, consistent with the larger unit cell of the PtSn alloy. EDX analysis gives a $Pt_{48}Sn_{52}$ average composition for the particles, which is almost identical to that of intermetallic NPs (Figure S2) and the precursor composition. The PtSn alloy catalysts were also made by depositing the as-prepared particles onto a carbon support, but no further heat treatments were used since PVP is weakly bound to the particle surface.

The PtSn@Pt core–shell NPs were prepared by CO-induced surface segregation of the PtSn intermetallic NPs (Scheme 1).[7] Specifically, a thin film of PtSn intermetallic

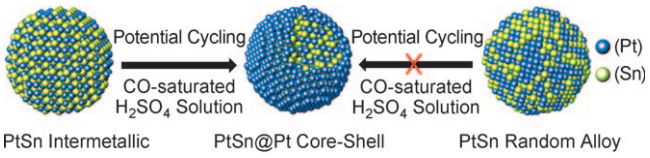

Scheme 1. Preparation of PtSn@Pt core–shell NPs from PtSn intermetallic NPs by potential cycling in CO-saturated H_2SO_4 solution.

catalyst was first made by depositing the carbon-supported intermetallic catalyst ink on a rotating disk electrode (RDE), followed by slow drying in air. The electrode was then subjected to potential cycling between −0.245 V and 0.5 V (vs. SCE) for 200 scans in CO-saturated 0.5 M H_2SO_4 solution. Owing to the strong adsorption of CO on Pt, CO segregated the Pt atoms to the particle surface during the potential cycling, thus forming PtSn@Pt core–shell type nanostructures. Note that potential cycling without CO presence does not induce core–shell formation. Figure 2a shows a representative TEM-EDX line scan of one PtSn@Pt core–shell NP. The presence of both Pt and Sn confirms the particles' bimetallic nature and the lack of complete phase separation into monometallic Pt and Sn (or SnO_x) NPs. The Pt distributions across the particles show Pt-rich edges relative to the core, which is characteristic of M@Pt core–shell NPs[6b,d] and is distinct from the Gaussian distributions observed for Pt in the alloy and intermetallic NPs (e.g. Figure 1d). In contrast to the bimodal Pt distributions, the Sn concentrations in the PtSn@Pt core-shell NPs still show nearly Gaussian distributions across the particles (Figure 2a). The XRD profiles of the PtSn@Pt core–shell NPs (Figure 2b) are dominated by the diffraction of the fcc Pt shells, but the slight lattice expansion of Pt in the shell structure causes the peaks to shift to lower angles.[6e] The XRD data also clearly show PtSn intermetallic diffraction peaks, indicating that the core retains its PtSn intermetallic structure. Based on the TEM-EDX line scans, XRD study and electrochemical data (see below), it is clear that the PtSn intermetallic NPs convert to PtSn@Pt core–shell architectures after the potential cycling process. TEM and EDX studies do not show significant changes of particle size and composition during the architectural transformation (Figure S3). However, it is likely that a small amount of Sn dissolution occurs during the process, which allows for Pt shell formation while maintaining the PtSn core.

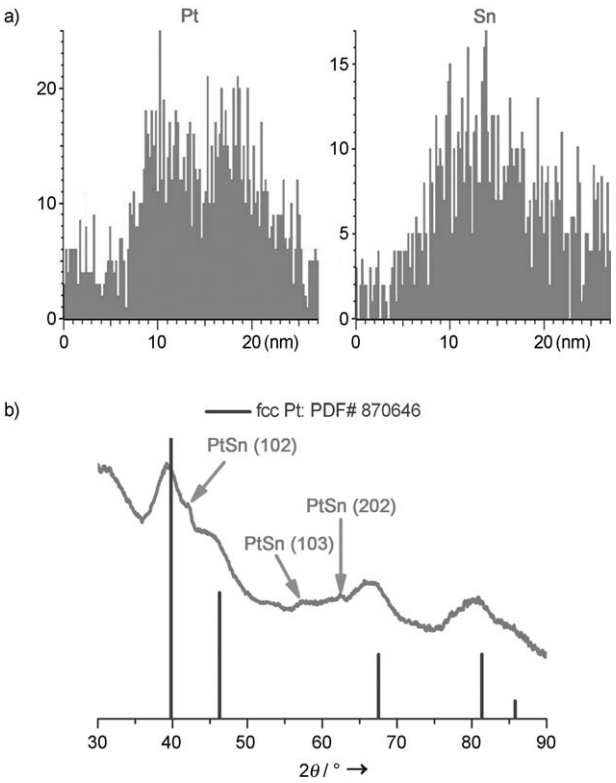

Figure 2. a) TEM-EDX line scan and b) XRD profile of PtSn@Pt core–shell NPs.

For direct comparison of their electrochemical properties, the PtSn intermetallic and PtSn random alloy catalysts were subjected to 200 potential scan cycles between −0.245 V and 0.5 V (vs. SCE) before data collection. However, the electrolyte was saturated with Ar instead of CO during this conditioning process. Figure 3 shows the CO stripping

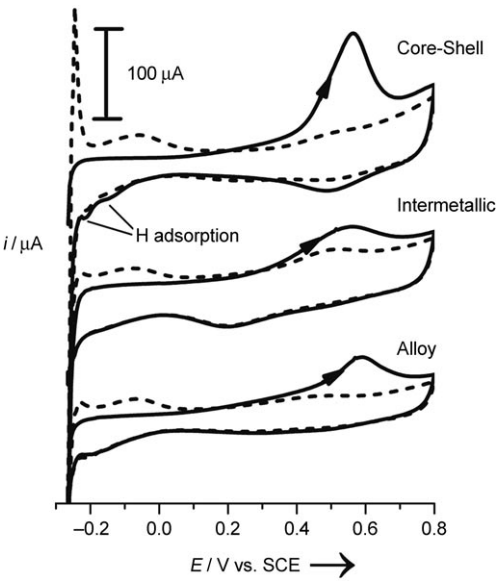

Figure 3. CO stripping curves of PtSn@Pt core–shell and PtSn intermetallic and PtSn alloy catalysts in 0.5 M H_2SO_4. Scan rate: 20 $mV s^{-1}$, $T = 298$ K. The dotted curves are the CVs recorded after CO stripping.

curves of these three catalysts. As expected, the intermetallic catalyst exhibits a broad CO oxidation peak since Sn is still present on the particle surface after the potential cycling. The presence of surface Sn is evidenced by the Sn oxidation peak at 0.5 V in the cyclic voltammogram (CV) after the CO stripping experiment (Figure 3, dotted line). The broad CO oxidation peak is associated with two types of CO_{ads} species on PtSn surface: one weakly adsorbed CO on Pt sites adjacent to Sn, and the other strongly adsorbed CO on Pt sites.[8] The CO oxidation at the lower potential is mainly associated with the weakly adsorbed CO. In contrast, both the alloy and core–shell catalysts show sharper, more "Pt-like" CO stripping curves compared to the intermetallic catalyst. For the PtSn alloy, the Pt-like feature shown in the CO-stripping curve is suggestive of a Pt-rich surface. The lack of a Sn oxidation peak in the CV of the PtSn alloy shows that Sn is not present on the NP surface. Due to the poor stability of PtSn alloy in the acidic electrolyte, a considerable amount of Sn dissolves during the potential cycling process. The RDE experiments suggest that the PtSn alloy actually converts to essentially a pure Pt NP after the potential cycling, as discussed below.

For the PtSn@Pt core–shell NPs, the sharp CO stripping peak indicates that the surface is covered by Pt. The integrated charge under the CO stripping region is approximately 2.5 times greater than that for the PtSn intermetallic, consistent with the displacement of surface Sn atoms by Pt during the potential cycling in CO-saturated solutions. The two well-defined H adsorption peaks characteristic of a pure Pt surface, as well as the absence of a Sn oxidation peak in the CV, provide additional evidence for a pure Pt surface in the PtSn@Pt NPs.

The CO tolerance of each catalyst was evaluated by thin-film RDE experiments. Figure 4 shows the polarization curves for electrooxidation of CO/H_2 mixtures (1000 ppm of CO) for five different catalysts. Compared to commercial E-TEK Pt and PtRu alloy catalysts, both the intermetallic and core–shell catalysts had much lower overpotentials for CO/H_2 oxidation, while the alloy exhibited a CO tolerance close to that of pure Pt. The CO/H_2 oxidation overpotential for the PtSn@Pt catalyst is cathodically shifted by ca. 200 mV and ca. 100 mV compared to those of Pt and PtRu, respectively. The remarkable CO tolerance of core–shell and intermetallic NPs is further evidenced by their low onset potentials for CO/H_2 oxidation, which start at as low as −0.15 V for core–shell and −0.05 V for intermetallic, compared to 0.05 V and 0.15 V for PtRu and Pt, respectively (Figure 4). The relatively low onset potential (ca. 0 V) for the PtSn alloy is probably associated with trace amounts of Sn remaining on the particle surface, where $Sn{-}OH_{ads}$ acts as an active site for the oxidation of $Pt{-}CO_{ads}$.[9] More significant, the PtSn@Pt catalysts show superior CO-tolerance relative to the PtSn intermetallic catalysts, exhibiting an additional 75 mV negative shift in CO/H_2 oxidation overpotential. The enhanced CO-tolerance of the core–shell NPs over the intermetallic NPs suggests the architectures have a significant impact on their reactivity. It is known that the "bifunctional mechanism" plays an important role in promoting CO-tolerance in PtSn alloys and intermetallics.[9] However, this mechanism cannot be operative for the core–shell catalyst due to the lack of surface Sn. The high CO-tolerance for the PtSn@Pt catalyst suggests that the electronic effect[10] associated with the core–shell structure may be more effective in promoting CO electrooxidation than the traditional bifunctional process. As with other core–shell nanostructures,[6a,b] the PtSn intermetallic core can modify the electronic structure of the Pt shell by shifting the d-band center of Pt,[11] thus promoting the electrooxidation process.

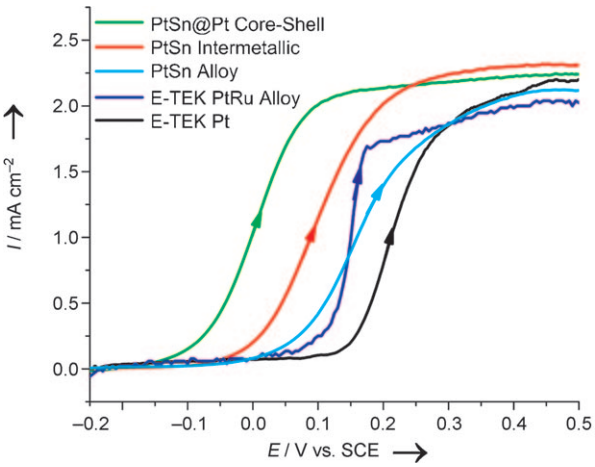

Figure 4. Polarization curves for electrooxidation of CO/H_2 mixtures (1000 ppm CO, balance H_2) on different Pt–Sn catalysts with comparisons to E-TEK Pt and PtRu catalysts (all catalysts contain 30% total metal loading). Curves were recorded at 298 K with 1 $mV s^{-1}$ scan rates and 1600 rpm rotation rates. Electrolyte: 0.5 M H_2SO_4 solution.

The relatively high stability of PtSn intermetallic NPs[5c,e] is critical for the preparation of PtSn@Pt core–shell NPs in acidic electrolytes. Attempts to use the PtSn random alloy to make core–shell NPs through potential cycling in CO-saturated H_2SO_4 solutions resulted in almost complete dissolution of Sn. Significant quantities of Sn^{2+}(aq) were apparent in the electrolytes used for the PtSn alloy catalysts (RDE and CV experiments) but Sn^{2+}(aq) was not detected in the electrolytes of the other catalysts. Moreover, the CO-tolerance of the PtSn alloy after the potential cycling in CO-saturated H_2SO_4 solutions is unchanged from that of the original catalyst (Figure S4). Note that PVP on the alloy NPs may slightly affect the current density but should not significantly affect the onset potential for CO/H_2 oxidation shown in Figure 4.

In summary, we have successfully prepared PtSn intermetallic and alloy NPs by chemical reduction routes. PtSn@Pt core–shell NP electrocatalysts were made through potential cycling of PtSn intermetallic NPs in CO-saturated H_2SO_4 solutions. The relatively high chemical stability of the PtSn intermetallic relative to the PtSn alloy was found to be the key to the formation of core–shell nanostructures. Thin-film RDE tests demonstrated that the Pt@PtSn core–shell and the PtSn intermetallic electrocatalysts have substantially higher CO-tolerance compared to Pt, PtRu alloy, and PtSn alloy catalysts. We believe that the superior CO-tolerance of the PtSn@Pt catalyst is mainly due to the electronic effect of the PtSn core on the Pt shell, while the high CO-tolerance of the intermetallic is due to the bifunctional mechanism.

Experimental Section

PtSn intermetallic NPs were prepared by the co-reduction of [Pt(acac)$_2$] and $SnCl_4$ in octadecene by sodium triethylborohydride ($NaBEt_3H$). Specifically, [Pt(acac)$_2$] (40.0 mg) was first mixed with octadecene (10 mL), oleylamine (1.0 mL), and oleic acid (1.0 mL). The mixture was sonicated for ca. 10 min, and then $SnCl_4$ (12 μL) was added The obtained mixture was sonicated for another 30 min before it was transferred to a 50 mL flask and slowly heated to 120 °C. In another flask, octadecene (20 mL) was introduced and heated to 190 °C, and $NaBEt_3H$ (4.0 mL, 1.0 M) was injected (caution). Then, the hot solution of precursors was quickly injected into the flask containing $NaBEt_3H$ and octadecene. The obtained mixture was heated to 195 °C and was kept at this temperature for 1 h. Afterwards, the solution was cooled down to room temperature. Finally, the particles were washed with ethanol and precipitated by centrifugation. To make PtSn random alloy NPs, [Pt(acac)$_2$] (40.0 mg), $SnCl_4$ (12 μL), and PVP (100 mg) were added to a 100 mL flask containing dry ethylene glycol solution (30 mL). The mixture was heated to 185 °C and was kept at this temperature for 30 min. The particles were washed with acetone and precipitated by centrifugation.

To make carbon-supported PtSn intermetallic electrocatalysts with 30 wt % (total metal) loading, the as-prepared NPs dispersed in hexane were mixed with Vulcan XC-72 powder (73.3 mg) by sonication for 3 h. After sonication, the catalyst was dried in air with the evaporation of hexane. The dried catalyst was then subjected to heat treatment at 450 °C in Ar/H_2 (5 % of H_2) atmosphere for 2 h. Catalysts of PtSn random alloy were prepared by the similar method, but no heat treatments were used.

TEM and HRTEM images were obtained on a JEM 2100 LaB6 TEM operating at 200 kV. EDX and EDX line scan analysis was performed on a JEOL 2100F Field Emission TEM operating in the STEM mode. XRD patterns of samples were obtained on a Bruker C2 Discover (Parallel Beam) General Area Diffraction Detection (GADDS) system with a Bruker ACS Hi-Star detector. Electrochemical experiments were performed in a standard three-electrode electrochemical cell. A rotating disk electrode (glassy carbon) with dried catalyst ink on its surface was used as a working electrode. A Pt wire counter electrode and a saturated calomel electrode (SCE) reference electrode were used. All the potentials are reported with respect to SCE. The electrolyte was a 0.5 M H_2SO_4 solution. For potential cycling, the working electrode was scanned between −0.245 V–0.5 V in CO-saturated H_2SO_4 for 200 cycles with scan rate of 100 mV s^{-1}. After potential cycling, fresh electrolyte was used for acquiring the CO-stripping curves and polarization curves. In the CO-stripping experiments, the PtSn catalysts were saturated with CO by bubbling CO in the electrolyte for 10 min with the electrode potential held at −0.20 V vs. SCE, followed by argon-purging for 30 min. To obtain the polarization curves for electro-oxidation of H_2 in the presence of CO, the electrolyte was bubbled with CO/H_2 mixture (1000 ppm of CO) for 2 h with the electrode potential held at −0.20 V vs. SCE, followed by the potential scan at 1 mV s^{-1} with rotation rate of 1600 rpm.

Received: December 14, 2009
Published online: March 25, 2010

Keywords: alloys · core–shell structures · CO tolerance · intermetallic phases · PtSn nanoparticles

[1] a) E. Antolini, *J. Appl. Electrochem.* **2004**, *34*, 563; b) J. J. Baschuk, X. G. Li, *Int. J. Energy Res.* **2001**, *25*, 695; c) J. H. Wee, K. Y. Lee, *J. Power Sources* **2006**, *157*, 128; d) X. Cheng, Z. Shi, N. Glass, L. Zhang, J. J. Zhang, D. T. Song, Z. S. Liu, H. J. Wang, J. Shen, *J. Power Sources* **2007**, *165*, 739.

[2] a) T. J. Schmidt, M. Noeske, H. A. Gasteiger, R. J. Behm, P. Britz, H. Bönnemann, *J. Electrochem. Soc.* **1998**, *145*, 925; b) S. J. Lee, S. Mukerjee, E. A. Ticianelli, J. McBreen, *Electrochim. Acta* **1999**, *44*, 3283; c) P. Waszczuk, G. Q. Lu, A. Wieckowski, C. Lu, C. Rice, R. I. Masel, *Electrochim. Acta* **2002**, *47*, 3637; d) Z. L. Liu, X. Y. Ling, X. D. Su, J. Y. Lee, *J. Phys. Chem. B* **2004**, *108*, 8234; e) C. Bock, C. Paquet, M. Couillard, G. A. Botton, B. R. MacDougall, *J. Am. Chem. Soc.* **2004**, *126*, 8028; f) Z. Liu, E. T. Ada, M. Shamsuzzoha, G. B. Thompson, D. E. Nikles, *Chem. Mater.* **2006**, *18*, 4946.

[3] a) M. Arenz, V. Stamenkovic, B. B. Blizanac, K. J. J. Mayrhofer, N. M. Markovic, P. N. Ross, *J. Catal.* **2005**, *232*, 402; b) T. J. Schmidt, H. A. Gasteiger, R. Behm, *J. New Mater. Electrochem. Syst.* **1999**, *2*, 27; c) Z. Liu, D. Reed, G. Kwon, M. Shamsuzzoha, D. E. Nikles, *J. Phys. Chem. C* **2007**, *111*, 14223; d) L. H. Jiang, Z. H. Zhou, W. Z. Li, W. J. Zhou, S. Q. Song, H. Q. Li, G. Q. Sun, Q. Xin, *Energ. Fuels* **2004**, *18*, 866.

[4] a) S. Mukerjee, R. C. Urian, S. J. Lee, E. A. Ticianelli, J. McBreen, *J. Electrochem. Soc.* **2004**, *151*, A1094; b) S. Ball, A. Hodgkinson, G. Hoogers, S. Maniguet, D. Thompsett, B. Wong, *Electrochem. Solid-State Lett.* **2002**, *5*, A31; c) G. Papakonstantinou, F. Paloukis, A. Siokou, S. G. Neophytides, *J. Electrochem. Soc.* **2007**, *154*, B989.

[5] a) E. Casado-Rivera, D. J. Volpe, L. Alden, C. Lind, C. Downie, T. Vazquez-Alvarez, A. C. D. Angelo, F. J. DiSalvo, H. D. Abruna, *J. Am. Chem. Soc.* **2004**, *126*, 4043; b) H. Abe, F. Matsumoto, L. R. Alden, S. C. Warren, H. D. Abruna, F. J. DiSalvo, *J. Am. Chem. Soc.* **2008**, *130*, 5452; c) N. de-los-Santos-Álvarez, L. R. Alden, E. Rus, H. Wang, F. J. DiSalvo, H. D. Abruña, *J. Electroanal. Chem.* **2009**, *626*, 14; d) R. E. Cable, R. E. Schaak, *J. Am. Chem. Soc.* **2006**, *128*, 9588; e) J. C. Bauer, X. Chen, Q. S. Liu, T. H. Phan, R. E. Schaak, *J. Mater. Chem.* **2008**, *18*, 275.

[6] a) Z. Liu, J. E. Hu, Q. Wang, K. Gaskell, A. I. Frenkel, G. S. Jackson, B. Eichhorn, *J. Am. Chem. Soc.* **2009**, *131*, 6924; b) S. Alayoglu, A. U. Nilekar, M. Mavrikakis, B. Eichhorn, *Nat. Mater.* **2008**, *7*, 333; c) S. H. Zhou, B. Varughese, B. Eichhorn, G. Jackson, K. McIlwrath, *Angew. Chem.* **2005**, *117*, 4615; *Angew. Chem. Int. Ed.* **2005**, *44*, 4539; d) S. Alayoglu, B. Eichhorn, *J. Am. Chem. Soc.* **2008**, *130*, 17479; e) S. Alayoglu, P. Zavalij, B. Eichhorn, Q. Wang, A. I. Frenkel, P. Chupas, *Acs Nano* **2009**, *3*, 3127; f) S. R. Brankovic, J. X. Wang, R. R. Adzic, *Electrochem. Solid-State* **2001**, *4*, A217; g) M. Watanabe, H. Igarashi, T. Fujino, *Electrochemistry* **1999**, *67*, 1194.

[7] a) K. J. J. Mayrhofer, V. Juhart, K. Hartl, M. Hanzlik, M. Arenz, *Angew. Chem.* **2009**, *121*, 3581; *Angew. Chem. Int. Ed.* **2009**, *48*, 3529; b) F. Tao, M. E. Grass, Y. W. Zhang, D. R. Butcher, J. R. Renzas, Z. Liu, J. Y. Chung, B. S. Mun, M. Salmeron, G. A. Somorjai, *Science* **2008**, *322*, 932; c) R. Ferrando, J. Jellinek, R. L. Johnston, *Chem. Rev.* **2008**, *108*, 845; d) J. Nerlov, I. Chorkendorff, *J. Catal.* **1999**, *181*, 271; e) L. L. Wang, D. D. Johnson, *J. Am. Chem. Soc.* **2009**, *131*, 14023.

[8] a) N. M. Marković, B. N. Grgur, C. A. Lucas, P. N. Ross, *J. Phys. Chem. B* **1999**, *103*, 487; b) K. Wang, H. A. Gasteiger, N. M. Markovic, P. N. Ross, *Electrochim. Acta* **1996**, *41*, 2587.

[9] a) B. E. Hayden, M. E. Rendall, O. South, *J. Am. Chem. Soc.* **2003**, *125*, 7738; b) T. E. Shubina, M. T. M. Koper, *Electrochim. Acta* **2002**, *47*, 3621; c) W. J. Zhou, Z. H. Zhou, S. Q. Song, W. Z. Li, G. Q. Sun, P. Tsiakaras, Q. Xin, *Appl. Catal. B* **2003**, *46*, 273.

[10] a) M. Watanabe, Y. M. Zhu, H. Igarashi, H. Uchida, *Electrochemistry* **2000**, *68*, 244; b) H. Uchida, H. Ozuka, M. Watanabe, *Electrochim. Acta* **2002**, *47*, 3629; c) M. Watanabe, Y. M. Zhu, H. Uchida, *J. Phys. Chem. B* **2000**, *104*, 1762; d) M. Wakisaka, S. Mitsui, Y. Hirose, K. Kawashima, H. Uchida, M. Watanabe, *J. Phys. Chem. B* **2006**, *110*, 23489.

[11] a) B. Hammer, Y. Morikawa, J. K. Norskov, *Phys. Rev. Lett.* **1996**, *76*, 2141; b) B. Hammer, J. K. Norskov, *Adv. Catal.* **2000**, *45*, 71.

